ISSN 1027-4510, Journal of Surface Investigation. X-ray, Synchrotron and Neutron Techniques, 2012, Vol. 6, No. 4, pp. 668–672. © Pleiades Publishing, Ltd., 2012.
Original Russian Text © A.F. Zatsepin, E.A. Buntov, V.S. Kortov, V.A. Pustovarov, H.-J. Fitting, B. Schmidt, N.V. Gavrilov, 2012, published in Poverkhnost'. Rentgenovskie, Sinkhrotronnye i Neitronnye Issledovaniya, 2012, No. 8, pp. 44–49.

Low-Temperature Photoluminescence of Ion-Implanted SiO_2:Sn^+ Films and Glasses

A. F. Zatsepin[a], E. A. Buntov[a], V. S. Kortov[a], V. A. Pustovarov[a], H.-J. Fitting[b], B. Schmidt[c], and N. V. Gavrilov[d]

[a] *Ural Federal University, ul. Mira 19, Yekaterinburg, 620002 Russia*
[b] *Institute of Physics, University of Rostock, Universitätsplatz 3, D-18051 Rostock, Germany*
[c] *Institute of Ion Beam Physics and Materials Research, D-01314, Dresden, Germany*
[d] *Institute of Electrophysics, Ural Branch, Russian Academy of Sciences, ul. Amundsena 106, Yekaterinburg, 620016 Russia*

Received December 27, 2011

Abstract—Low-temperature photoluminescence spectroscopy with pulsed synchrotron excitation is applied to study the regularities of excitation and relaxation of both point defects and nanoparticles formed by tin implantation into SiO_2 films and glasses. It has been found that tin implantation followed by air and nitrogen annealing yields the formation of α-Sn nanoclusters and nonstoichiometric SnO_x nanoparticles, while a stable phase of SnO_2 does not appear. Alternative channels of luminescence excitation are revealed for nanoclusters, including energy transfer from excitons and electron–hole pairs of the host SiO_2 matrix.

DOI: 10.1134/S1027451012080198

INTRODUCTION

A study of the luminescent properties of semiconductor nanoparticles implanted into dielectric matrices are of interest in connection with the development of promising functional structures for micro-, opto-, and nanoelectronics. In particular, such characteristics as photosensitivity and luminescence ability are important for materials and elements of fiber and waveguide technology [1, 2, 3].

Recent investigations show that ion implantation of IV group elements into SiO_2-based bulk glasses and thin films yields the formation of structures that are luminescent in the visible and ultraviolet spectral ranges [4, 6]. The implantation of tin ions into a matrix of silicon dioxide results in the formation of nanocrystals of α-Sn [7] and oxidized SnO_2 nanoparticles [8, 9], which cause serious complications in understanding the optical properties of the obtained nanocomposites.

Different models have been used to describe the photoinduced phenomena in implanted glasses and films [10–13]. However, there are many problems concerning the nature and the energy structure of luminescence centers, features of their excitation, and regularities and mechanisms of the radiative processes in nanostructured systems of the SiO_2:Sn type that remain unsolved. The main reason for this is as follows: the photoluminescence of implanted systems is usually studied using laser excitation, which yields rather limited information on both the nature and the properties of excited states of luminescent nanoparticles and clusters. In contrast, selective excitation of luminescence by synchrotron radiation allows the identification of different energy transfer channels in a nanocluster–matrix system [14], while the use of cryogenic temperatures allows detailed information on the physical nature and structure of luminescence centers to be obtained thanks to the low probability of nonradiative electronic-vibrational transitions.

Taking the above said into account, the aim of this paper is to study the features of excitation and spectral-kinetic characteristics of the low-temperature photoluminescence (PL) of implanted SiO_2:Sn^+ films and glasses using synchrotron radiation.

OBJECT AND METHOD OF THE EXPERIMENT

The main objects of study were SiO_2 films (500 nm thick) thermally grown on a silicon substrate irradiated with Sn^+ ions ($E = 400$ keV, $\Phi = 5 \times 10^{16}$ cm^{-2}) and annealed at $T = 900$°C for one hour in an atmosphere of dry nitrogen. Quartz glasses (KU grade) implanted with Sn^+ ($E = 30$ keV, $\Phi = 5 \times 10^{16}$ cm^{-2}, and annealed at $T = 900$°C in the air) were used for comparative analysis and interpretation of the nature of luminescence centers. Irradiation with tin was performed in the pulsed-periodic mode with a pulse duration of 0.4 ms and a frequency of 25 Hz. The beam current density in the pulse was 0.6 mA/cm^2. For the implanted samples to be calibrated with the RENISHAW spectrometer, the spectra of Raman light scattering (RSS) excited by the 514 nm line of an argon laser focused onto an area 2 μm in diameter were recorded.

The luminescence spectra in the range of 1.5–6.0 eV, the PL excitation spectra (3.7–16 eV), and the kinematic curves were recorded during selective VUV-excitation (vacuum ultra-violet) at the SUPERLUMI station of the DESY synchrotron (Hamburg, Germany). The photoluminescence spectra were recorded with the help of a 0.3-m ARC Spectra Pro-308i monochromator and an R6358P multiplier (Hamamatsu) in two time intervals, namely, $\Delta t_1 = 11.8$ ns (the fast component) and $\Delta t_2 = 92$ ns (the slow component), which were shifted with respect to the beginning of the excitation pulse by $\delta t_1 = 2.7$ ns and $\delta t_2 = 60$ ns, respectively. The excitation spectra were normalized to an equal number of exciting photons using sodium salicylate. The components of the PL kinetics were analyzed using the method of inverse convolution.

RESULTS AND DISCUSSION

RSS Spectra

Figure 1 shows the Raman scattering spectra of the analyzed films and glasses. It can be seen that the RSS spectra for annealed films of SiO_2:Sn^+ coincide, on the whole, with those for nonimplanted films (Fig. 1a). The maxima (520 and 300 cm^{-1}) caused by the influence of the silicon substrate are predominant. In the initial and irradiated glasses (Fig. 1b), one can see the known vibrational peaks of silicon dioxide: the D_1 and D_2 bands at 490 and 610 cm^{-1} are related to the symmetric extension modes of the vibration-isolated three- and four-link rings of the SiO_4 tetrahedrons [15], a 440 cm^{-1} band ascribed to the symmetric extension mode ω_1, and a maximum at 800 cm^{-1} corresponding to the ω_2 mode [16, 17].

It follows from Fig. 1 that the most noticeable effect of ion implantation is an increase in the intensity of the RSS maxima in the range of 100–200 cm^{-1}. In this case, one can observe a redistribution of the intensity between the above peak and other spectral maxima. Note that in previous studies [7, 18] an increase in the intensity of low-frequency vibrations during the implantation of tin was not recorded due to the limitation of the spectral range of the RSS recording. It was shown in [19, 20] that the 630 cm^{-1} band (A_{1g} mode) in the high frequency range can serve as an indicator of SnO_2 phase formation, while a low-frequency 275 cm^{-1} mode characterizes the formation of nonstoichiometric nanoparticles of $SnO_{1.5}$ [18].

In our case, the A_{1g} mode hardly appears in the RSS spectra of implanted KU glasses, which points to a negligible number of oxidized nanoparticles directly formed during implantation (Fig. 1). Subsequent thermal treatment also does not increase their number. At the same time, at least two elementary bands in the low-frequency range (123 and 190 cm^{-1}) can be distinguished in the glass spectra. In this case, the implanted films also demonstrate a low-frequency peak at 115 cm^{-1}, which can be partially distorted by its proximity to the sensitivity limit of the device. In

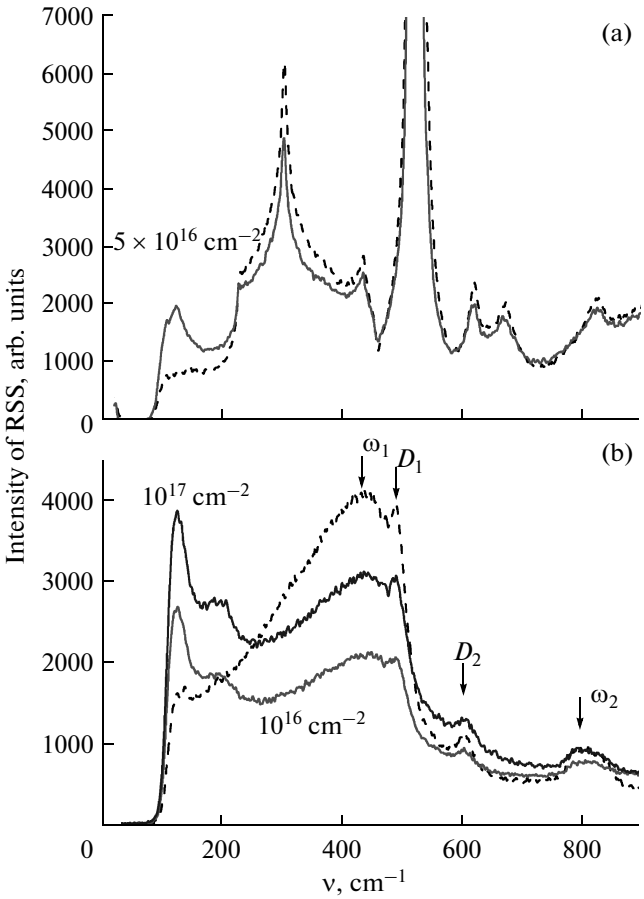

Fig. 1. Raman scattering spectra of the initial (dashed line) and implanted (solid line) (a) SiO_2 films and (b) quartz glasses with Sn^+ 10^{16} and 10^{17} cm^{-2} fluences recorded at room temperature. The implanted samples were annealed at a temperature of 900°C.

principle, the revealed features in the RSS spectra can be caused by both the formation of tin nanoclusters and distortion of the vibrational spectrum of the SiO_2 oxide matrix due to the implantation of heavier tin atoms into the lattice. However, taking into account dose variations of the intrinsic D_1 and D_2 bands of the amorphous matrix, interpreted within the framework of the densification model [11], the last version should be considered more preferable.

Photoluminescence Spectra

The photoluminescence spectra of the initial films contain weak bands of oxygen-deficiency centers at 2.5–3.5 and 4.3–4.5 eV [21]. After implantation of Sn^+ ions followed by annealing, the luminescent properties of the films significantly change. Special attention should be paid to the fact that, similar to the effect of laser and cathode action, photon irradiation in the VUV-range with the energy of 11 eV excites a whole series of luminescence bands, The maximum at 2.6 eV is related to intrinsic luminescence of autolocalized

Spectral parameters of the PL bands of implanted SiO_2:Sn films and glasses

Matrix	Parameter	α-Sn	nc-Si	nc-Sn	ALE	SnO_x	Sn-ODC
Film	$h\nu_m$, eV	1.55	1.74	2.05	2.58	3.33	4.07
	FWHM*, eV	0.18	0.20	0.41	0.37	0.48	0.53
Glass	$h\nu_m$, eV	1.65	1.86	2.11	2.47	2.90	–
	FWHM*, eV	0.16	0.12	0.26	0.40	0.58	–

* Full width at half maximum.

excitons (ALEs) of SiO_2. Intense PL maxima are observed at 1.6, 3.25, and 2.5 eV; two weak maxima are observed at 2.1 and 4.0 eV (Fig. 1a, Table). The spectral characteristics of the 3.25- and 4.0-eV bands correspond to the singlet–singlet radiative transitions of a tin-containing modification of oxygen-deficiency centers (Sn-ODC) [12, 13]. There are different ODC models for undoped SiO_2, namely a neutral oxygen vacancy ≡Si–Si≡ and a double-coordinated atom of silicon Si_2^0 [22]. In principle, three versions of Sn-ODC formed by substitution of silicon for a tin atom (namely ≡Sn–Si≡, ≡Sn–Sn≡, and Sn_2^0) can exist in the implanted SiO_2. An intense 3.3-eV band technically falls into the spectral range of triplet ODC luminescence. However, its nature cannot be caused by the triplet–singlet radiative transition of ODC-defects, since the probability of such transitions at liquid helium temperatures is close to zero. We suspect that the 3.3-eV luminescence band in implanted SiO_2 films and glasses is related to the presence of partially oxidized nonstoichiometric (by oxygen) SnO_x nanoparticles for which the value of the x nonstoichiometry parameter depends on the mode and atmosphere of thermal annealing.

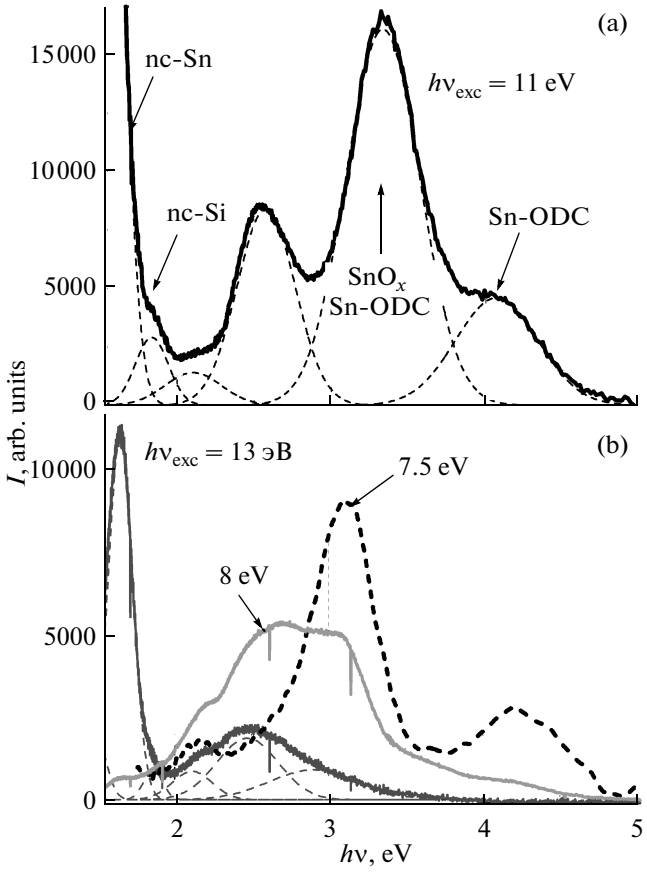

Fig. 2. PL spectra (500 nm) of the (a) implanted films and (b) quartz glasses before (dashed line) and after (solid line) annealing; recorded at a temperature of 10 K.

A rather intense 1.6-eV band appears in implanted SiO_2 glasses and films only after thermal annealing (Figs. 2a and 2b) against the background of the weakening PL of the oxygen-deficiency Sn-ODC centers. A feature of the 1.6-eV band behavior is as follows: it is observed at excitation energies over 10 eV, and a further energy increase simultaneously yields weakening of the PL maxima in the range of 2–4 eV. Recording of the 1.6-eV band in implanted glassy and thin-film SiO_2 samples allows its physical nature to be interpreted as luminescence of spatially limited excitons in tin nanoclusters (α-Sn). The calculations [4] show that the energy gap for α-tin can vary (depending on the cluster size) within the range from zero (bulk tin) to 2.5 eV (nanostructure). In our case, the radiation energy in the 1.6-eV band corresponds to the mean radius R of α-Sn nanoclusters no larger than 5 nm. A weak maximum in the range of 1.7–1.8 eV observed in the PL spectrum of implanted films can be caused by the luminescence of clustered silicon atoms [14]. In the near spectral range of about 1.9 eV, one can observe the luminescence of the centers of unbridged oxygen (NBOHC) in the irradiated SiO_2 matrices; however they are unlikely to appear in films and glasses with a significant concentration of OH-groups.

Luminescence Excitation Spectra

As distinct from laser excitation, selective synchrotron excitation allows the implementation of different channels of PL excitation in a broad energy range up to 40 eV. The excitation spectra for the majority of PL bands of the implanted samples are very complicated in shape with the most pronounced maxima at 5.0–5.5, 10, and 12 eV (Fig. 3). The experimental data

show that the most effective PL excitation is observed as a result of the nonradiative transfer of energy from the housing SiO_2 matrix to the luminescence spectra. The spectral range can be conveniently divided into three regions corresponding to the excitation of the intracenter luminescence of point defects, excitons, and electron–hole pairs of SiO_2.

The effects of optical excitation in a "matrix–cluster" system were previously observed for films implanted with silicon [16]. It has been shown that the most effective excitation of silicon-cluster luminescence occurs when the energy of the primary photons is comparable with or exceeds the width of the band gap of the SiO_2 matrix. At the same time it is known [23] that when amorphous SiO_2 is irradiated with high-energy photons ($h\nu > 11$ eV), the preferred autolocalization of holes (ALH) takes place. This implies that the energy transfer mechanism in the region of interzone transitions should include stages of hole localization and subsequent recombination of free electrons at them.

Excitation in the intermediate range of 8.5–11 eV corresponds to active generation of SiO_2 excitons. In particular, a 10.4-eV exciton band of optical absorption (whose interpretation still remains disputable) is well known for amorphous silicon dioxide. Some authors [24] distinguish several overlapping maxima in this spectral range corresponding to different types of excitons depending on their mobility. At the same time, recent investigations of the reflection spectra of glassy SiO_2 (Suprasil F300, type IV) in the VUV range [25, 26] point to the elementary character of the Lorentz shape of the 10.4-eV absorption band in a broad temperature range, which indicates increased mobility of the formed excitons. In our case, the nonsymmetric shape of the 10.2-eV band in the FLV spectra of SnO_x nanoparticles and α-Sn nanoclusters points to the participation of both free and autolocalized excitons in the excitation processes . In this case, mobile excitons transfer their energy to luminescence centers during the process of migration, while a resonance-transfer mechanism can take place for localized excitons.

As distinct from nanoparticles, oxygen-deficiency centers of Sn-ODC demonstrate exclusively resonant excitation through the singlet states S_1 and S_2 (Fig. 3b). Correlation between the 4-eV band and singlet ODC luminescence is additionally confirmed by kinetic measurements. The damping curves of this band in a film and glass (Fig. 4) are well described by an exponential function of the nanosecond range with lifetimes of 4.5 and 9.3 ns, respectively. The first value is close to the analogous parameter of the singlet Sn-ODC luminescence in the sol–gel SiO_2 glass [27]. Thus, the 3.2-eV luminescence band in unannealed glass (microsecond kinetics) and the 4.1-eV band ($\tau =$ 4.5 ns) are interpreted by us based on the spectral position and lifetimes as triplet–singlet and singlet–singlet

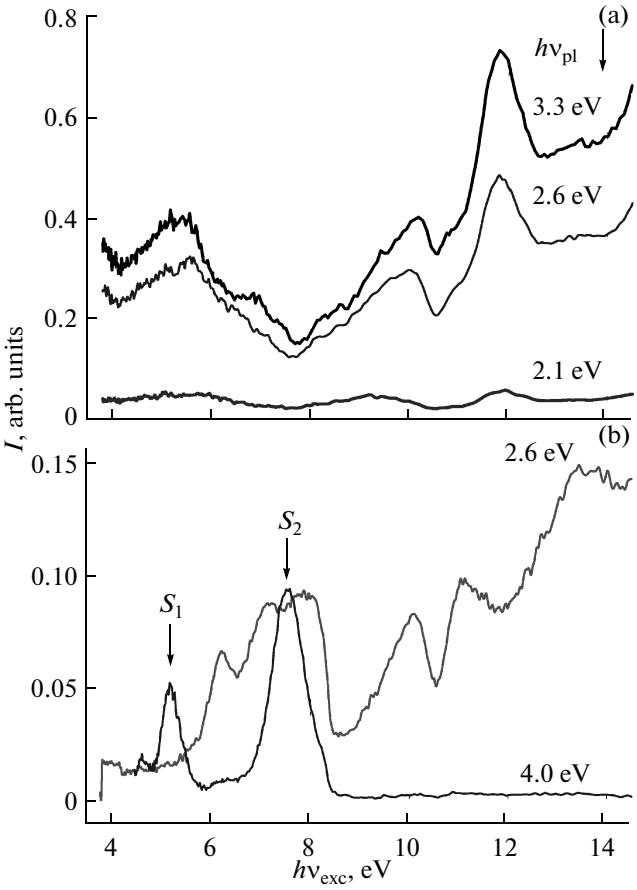

Fig. 3. Excitation spectra of the observed PL bands for (a) the implanted films and (b) glasses; S_1 and S_2 are the first and the second excited states of Sn-ODC.

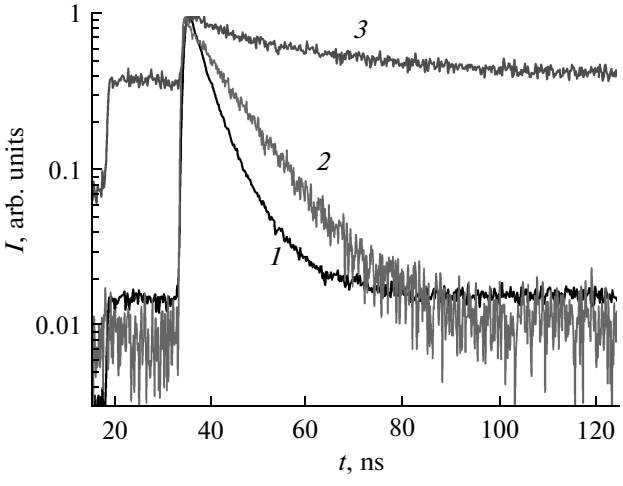

Fig. 4. Kinetics of the "fast" PL bands (2.12, 4.0 eV) of the SiO_2-Sn^+ samples at an excitation energy of 11 eV. (*1, 2*) the 4-eV band (resonant excitation is 7.5 eV; the lifetime is 4.5 and 9.3 ns for the film and glass, respectively); (*3*) the 2.1-eV band (exciton excitation of 11 eV; $\tau = 24$ ns.

radiative transitions in oxygen-deficiency centers of the Sn-ODC type [13, 27].

The luminescence of silicon nanoparticles is usually characterized by slow micro- and millisecond kinetics. An analogous situation takes place for the PL maxima of 1.6, 1.8, and 3.3 eV in annealed SiO_2:Sn glasses and films. However, the radiation in the 2.1-eV range which is sometimes associated with the luminescence of small-size clusters of tin demonstrates a short lifetime ($\tau = 24$ ns). Interpretation of this band, with the significant difference in kinetics as compared to the 1.6-eV band, necessitates additional studies.

On the whole, it is possible to believe that implantation of tin ions followed by thermal treatment substantially affects the structure of the silicon–oxygen matrix and yields the formation of luminescent nanosized α-Sn clusters, oxidized SnO_x nanoparticles, and radiation damages of the lattice of the type of silicon and oxygen displaced atoms. Thermal treatment yields the release and growth of tin-containing nanoinclusions and partial annealing of luminescent defects.

CONCLUSIONS

Regularities of the excitation and relaxation of implanted defects and nanoparticles in ion-modified SiO_2:Sn^+ films and glasses at helium temperatures were investigated using the technique of photoluminescence spectroscopy with pulsed synchrotron excitation. It has been revealed that implantation of tin followed by annealing in a nitrogen and air atmosphere yields the formation of α-Sn nanoclusters, while a stable phase of SnO_2 is not formed. The appearance of high-energy PL bands also points to the formation of partially oxidized nonstoichiometric SnO_x nanoparticles. The degree of particle oxidation depends on the annealing temperature, duration, and atmosphere.

The intense long-wave PL bands of the analyzed samples are ascribed to nanosized clusters of α-tin formed as a result of implantation and thermal annealings. Alternative channels for cluster luminescence excitation with the participation of point defects, excitons, and electron–hole pairs of the SiO_2 matrix have been revealed. The most effective channel for cluster luminescence excitation is the transfer of energy from excitons and electron–hole pairs of the oxide matrix, which correspond to intense 10- and 12-eV excitation bands. At the same time, oxygen-deficiency centers demonstrate exclusively resonant excitation within the limits of the SiO_2 band gap.

REFERENCES

1. K. O. Hill and G. Meltz, J. Lightwave Tech. **15**, 1263 (1997).
2. G. Brambilla, V. Pruneri, and L. Reekie, Appl. Phys. 1 Lett. **76**, 807 (2000).
3. B. Poumellec and F. Kherbouche, J. Phys. III **6**, 1595 (1996).
4. S. Huang, Y. Chen, H. Xiao, and F. Lu, Surf. Coat. Technol. **205**, 2247 (2010).
5. A. F. Zatsepin, V. S. Kortov, N. V. Gavrilov, and D. Yu. Biryukov, J. Surf. Invest. **2**, 450 (2008).
6. V. S. Kortov, A. F. Zatsepin, D. Yu. Biryukov, and B. Schmidt, Poverkhnost', No. 7, 84 (2006).
7. P. K. Kuiri, H. P. Lenka, J. Ghatak, G. Sahu, B. Joseph, and D. P. Mahapatra, J. Appl. Phys. **102**, 024315 (2007).
8. M. A. Tagliente, V. Bello, G. Pellegrini, G. Mattei, P. Mazzoldi, and M. Massaro, J. Appl. Phys. **106**, 104304 (2009).
9. M. A. Tagliente, V. Bello, G. Pellegrini, G. Mattei, P. Mazzoldi, M. Massaro, and D. Carbone, Nucl. Instrum. Methods. Phys. Res. B **268**, 3063 (2010).
10. R. M. Atkins, V. Mizrahi, and T. Erdogan, Electron. Lett. **29**, 385 (1993).
11. M. G. Seats, G. R. Atkins, and S. B. Poole, Ann. Rev. Mater. Sci. **23**, 381 (1993).
12. J. M. J. Lopes, F. Kremer, P. F. P. Fichtner, and F. C. Zawislak, Nucl. Instrum. Methods. Phys. Res. B **242**, 157 (2006).
13. L. Rebohle, J. von Borany, and H. Frob, Nucl. Instrum. Methods. Phys. Res. B **188**, 28 (2002).
14. A. F. Zatsepin, V. S. Kortov, V. A. Pustovarov, E. A. Buntov, and H.-J. Fitting, J. Non-Cryst. Solids **355**, 1119 (2009).
15. F. L. Galeener, Solid State Commun. **44**, 1037 (1982).
16. F. L. Galeener, Phys. Rev. B **19**, 4292 (1978).
17. R. A. Murray and W. Y. Ching, Phys. Rev. B **39**, 1320 (1989).
18. C. Meier, S. Luttjohann, and V. G. Kravets, J. Appl. Phys. **99**, 113108 (2006).
19. R. S. Katiyar, P. Dawson, M. M. Hargreave, and G. R. Wilkinson, J. Phys. C: Solid State Phys. **4**, 2421 (1971).
20. S. G. Ansari, M. A. Dar, M. S. Dhage, Y. S. Kim, Z. A. Ansari, A. Al-Hajry, and H.-S. Shin, Rev. Sci. Instrum. **80**, 045112 (2009).
21. A. F. Zatsepin, H.-J. Fitting, V. S. Kortov, V. A. Pustovarov, B. Schmidt, and E. A. Buntov, J. Non-Cryst. Solids **355**, 61 (2009).
22. L. Skuja, J. Non-Cryst. Solids **239**, 16 (1998).
23. D. L. Griscom, Phys. Rev. B **40**, 4224 (1989).
24. A. N. Trukhin, J. Non-Cryst. Solids **149**, 32 (1992).
25. F. Messina, E. Vella, M. Cannas, and R. Boscaino, Phys. Rev. Lett. **105**, 116401 (2010).
26. E. Vella, F. Messina, M. Cannas, and R. Boscaino, Phys. Rev. B **83**, 174201 (2011).
27. M. D'Amico, F. Messina, M. Cannas, M. Leone, and R. Boscaino, J. Phys. Chem. A **112**, 12104 (2008).

SPELL: 1. ok